Journal of Nuclear Materials 393 (2009) 22–29

Contents lists available at ScienceDirect

Journal of Nuclear Materials

journal homepage: www.elsevier.com/locate/jnucmat

Young's modulus measurements of SiC coatings on spherical particles by using nanoindentation

J. Tan [a], P.J. Meadows [a], D. Zhang [b], Xi Chen [c], E. López-Honorato [a], X. Zhao [a], F. Yang [a], T. Abram [b], P. Xiao [a,*]

[a] School of Materials, University of Manchester, Manchester, M1 7HS, UK
[b] School of Mechanical, Aerospace and Civil Engineering, University of Manchester, UK
[c] Department of Civil Engineering and Engineering Mechanics, Columbia University, New York, USA

ARTICLE INFO

Article history:
Received 12 December 2008
Accepted 5 May 2009

ABSTRACT

Spherical silicon carbide coatings are deposited by fluidised bed chemical vapour deposition for the application to Tristructural Isotropic (TRISO) coated fuel particles. The silicon carbide exhibits columnar structure and grows along the radial direction during deposition. In this work, two measurements are made with nanoindentation, one is measured vertically to the grain growth direction, which gives a Young's modulus of 391.1 ± 12.9 GPa, and the other is measured along the grain growth direction which gives a Young's modulus of 442.5 ± 13.3 GPa. Finite element analysis and a theoretical effort are introduced to estimate the bending contribution when the indentation is carried out on the external surface of SiC. The relationship between grain orientation of SiC and its Young's modulus has been examined.

© 2009 Elsevier B.V. All rights reserved.

1. Introduction

In order to retain gas and metal fission products and enhance mechanical stability during irradiation, a silicon carbide coating is often applied to the Tristructural Isotropic (TRISO) coated fuel particles in the High Temperature Reactor [1,2]. Typically, the SiC coating is deposited on top of the pyrolitic carbon layer (PyC) by chemical vapour deposition (CVD), and the thickness of the spherical shell is around 35 μm (Fig. 1). Since silicon carbide is a brittle material, which acts as a pressure vessel in the coated fuel particles to withstand high stresses during irradiation, and the stress developed in the SiC is proportional to its Young's modulus, the knowledge of the Young's modulus (in both radial and transverse directions) is critical for the assessment of the mechanical integrity of the particles.

The mechanical properties of thin SiC films have been measured by various established methods, including brittle ring test [3–6], tensile testing [7], bending test [8], acoustic microscopy [9], micro-cantilever method [10] and indentation techniques. Among these methods (Table 1), tensile and bending test can be used to obtain the mechanical properties of a flat thin film but not a spherical film with an enclosed substrate. The brittle ring test was used to measure the Young's modulus of the entire or half SiC ring, which was made by double-side polishing and then burning carbon in the furnace, through compressing the ring between two sapphire plates [3,6]. Based on this test, the Young's modulus of a spherical SiC film was obtained between 300 and 600 GPa. The method is not accurate enough because the measured values would depend on the size of the ring. Micro-cantilever method is an accurate way of obtaining the modulus of SiC film, however the sample needs to be made by using a focused ion beam system (FIB) and then bent by using nanoindentation. The sample preparation is complex, which limits the scope of application of this technique [10].

Nanoindentation is an adaptable technique for thin spherical SiC film because it exhibits better reproducibility and convenience in measurements [9]. In nanoindentation, Young's modulus could be calculated by the load–displacement curves through the Oliver–Pharr method using the equation [11]

$$E_r = \frac{\sqrt{\pi}}{2} S \frac{1}{\beta} \frac{1}{\sqrt{A_c}} \tag{1.1}$$

where β is a constant equal to 1.034 for a Berkovich indenter, S is the contact stiffness, A_c is the projected contact area, and E_r is the reduced modulus, which combines modulus of both the indenter and specimen. Considering the properties of the diamond indenter, the reduced modulus could have the following relationship [11]

$$\frac{1}{E_r} = \frac{1-v^2}{E} + \frac{1-v_d^2}{E_d} \tag{1.2}$$

where E is the modulus of the specimen, E_d is the modulus of the diamond Berkovich indenter (~1140 GPa), and v is the Poisson ratio; in our experiments, the Poisson's ratio of the diamond indenter and the specimen (SiC) are 0.07 and 0.25, respectively.

When performing nanoindentation measurements on the SiC layer coated on the carbon layer, several effects should be removed in the procedure, such as so-called substrate effect, surface roughness and size effect [12], which could significantly affect the mea-

* Corresponding author. Tel.: +44 161 3065941; fax: +44 161 3063586.
E-mail address: ping.xiao@manchester.ac.uk (P. Xiao).

0022-3115/$ - see front matter © 2009 Elsevier B.V. All rights reserved.
doi:10.1016/j.jnucmat.2009.05.001

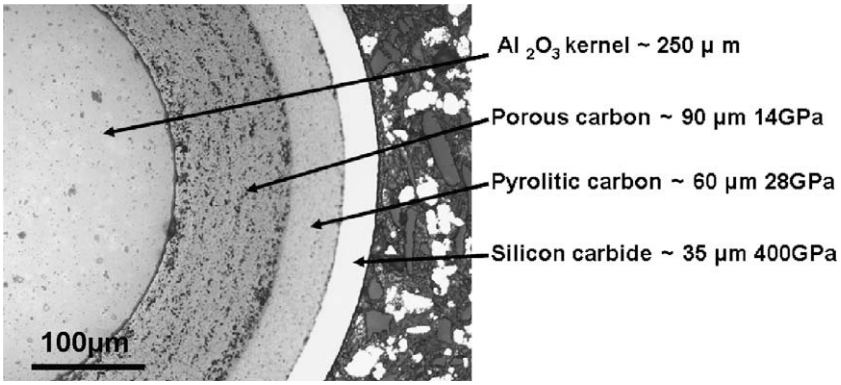

Fig. 1. The image of SiC and carbon layer in cross section of the coated particle.

Table 1
Some methods of modulus determination of SiC film.

Methods	Sample shape and size	Young's modulus (GPa)
Brittle ring test	SiC ring 30–80 μm thickness	300–600
Tensile test	Flat film 3.2 mm	421 ± 10
Bending test	Flat film on graphite disks 70–120 μm thickness	300–450
Acoustic microscopy	Flat film on plate substrate 15–60 μm thickness	434 ± 19

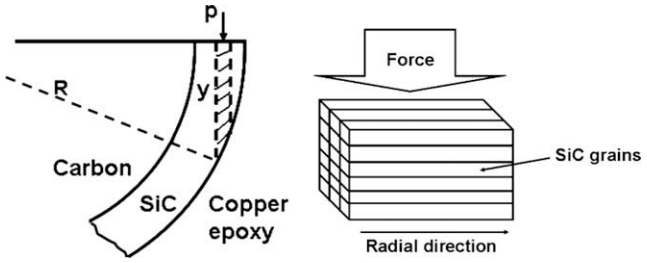

Fig. 2. The diagram of indentation in the cross section of SiC layer (left) and the schematic of indentation on the vertical grain growth direction (right) (The surrounding of SiC film is copper epoxy (its young modulus is 37 GPa), R – the radius of the whole particle, P – indentation force, y – the thickness of SiC under the indentation).

sured film properties. Among them, the surface roughness can be reduced through fine polishing while a fixed penetration depth is set to ignore the size effect for indentation. The substrate effect may be controlled by deformations of the film and substrate because the stresses transmit to the substrate via the thin film when the film thickness is low. Using finite element calculation, previous studies [13,14] showed that the surfaces of film and substrate near the indentation are depressed downward or sinking into the material even though the substrate was not in direct contact with the indenter. Chen and Vlassak [15] have discussed the substrate effect in the case of a soft film on a hard substrate and the case of a hard film on a soft substrate. In these cases, the measured mechanical properties are a combination of film and substrate properties. To avoid the substrate effect, the contact depths should be less than 10–20% of the film thickness, which is so-called one tenth rule. For some other film/substrate systems, for example, ultra-hard film on soft substrate, indentation experiments should be made within ~5% of the film thickness rather than 10% [16]. When the substrate is too soft to support the film, the bending effect would become a significant factor, and the measured values would be induced by both indentation and bending.

In this paper, the major objective is to measure the Young's modulus of the SiC layer in coated particles using indentation. Indentation was carried at both the cross-section and the external surface of the SiC layer after gentle polishing. Indentation on the cross-section of the SiC embedded in copper epoxy resin, allows measurements of Young's modulus of SiC vertical to the SiC CVD growth direction (Fig. 2). Finite element modelling is carried out to confirm that the copper epoxy resin used for embedding coated particles has little effect on indentation of SiC. Indentation on the external surface of the SiC (Fig. 3) should lead to measurements of Young's modulus of SiC along the SiC growth direction. However, indentations at the external surface of the SiC layer not only indent, but also bend the SiC layer. Therefore, finite element modelling is employed to simulate the bending effect of the SiC layer under indentation. The Young's modulus of SiC along the CVD grown direction is obtained based on the deconvolution of SiC layer bending and local indentation at the SiC surface.

2. Experiments

2.1. Materials

Both pyrocarbon layer (PyC) and silicon carbide layer (Fig. 1) are coated on alumina spherical particles from Brace GmbH Co. The pyrocarbon layer is deposited at 1250 °C from a mixture of ethyne and propene at 25 vol% while the silicon carbide layer is produced by methyltrichlorosilane (CH_3SiCl_3, MTS), by using fluidised bed chemical vapour deposition (FBCVD) at 1500 °C with 9.1 vol% MTS. Details on preparation of the coated particles are given in Ref. [17]. After deposition, the coated particles are embedded in copper epoxy resin from MetPrep Ltd. by using hot-pressing process. The embedded particles are polished to obtain a smooth surface by standard metallography procedures using SiC sand-paper, and then followed by diamond paste of 6, 1 μm in diameter. The surface roughness is controlled to be as small as 10 nm, measured by atomic force microscopy, which is much smaller than the contact depth (~300 nm in our experiment) and thus the roughness effect could be neglected. For the cross-section polishing (Fig. 1), the particles are polished into half spheres so that indentation can be performed perpendicular to the radial direction (Fig. 2).

In addition to indentation on the cross-section indentation of SiC layer, the polished outer spherical surface of SiC layer also needs to be carried out. On the external surface, the SiC coating is polished away several microns along the radial direction to produce a flat circular area on the external surface while the radius of the circle depends on the polished depth.

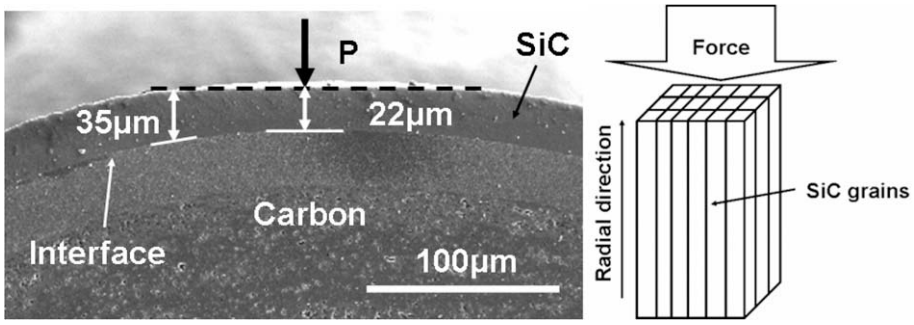

Fig. 3. Left: The SEM image of SiC layer polished from external surface (Here 13 μm are polished away) (Some white plots are due to carbon coating) Right: the diagram of indentation along grains.

The thickness of SiC varies with positions, the minimum thickness at the centre of circle is 22 μm and thickness of SiC layer is 35 μm in the particle (Fig. 3). Meanwhile, the SiC grain orientation varies with different positions as well.

2.2. Finite element analysis

The finite element (FE) calculation with ABAQUS software is first used to examine how the copper epoxy resin affects the indentation on SiC cross-section in coated particles, embedded in the copper epoxy. Because the indentation depth/radius is much smaller than the dimension (radius) of either the particle or the copper epoxy, the effect of curvature is ignored and the finite element model is simplified as a three-layered system (like a sandwich): PyC, SiC and Copper epoxy mounting compound. The dimensions ($x \times y \times z$) of these three layers are (a Y-symmetry boundary condition is applied on the y-plane) shown as Fig. 4. A homogenous SiC material is applied as a calibration to compare the results.

For indentation on the external surface of SiC, the FE calculation is applied to work out the bending effect. The structure of a coated particle is simplified as an inner solid sphere and an outer spherical shell with external surface flattened. A force of 133 mN used for nano indentation (Fig. 3), is applied to the centre of the circular flat area with the minimum thickness of 22 μm. To simplify the calculation, both SiC and PyC are assumed to be isotropic elastic. The FE model only simulates bending of the SiC layer. The dimensions and material properties of the models are shown in Table 2. It should be noted that the Young's moduli of both PyC and SiC are assumed as input data in order to simulate the bending displacement. The modulus of PyC is obtained by nanoindentation in the cross section. Such value should be reliable because the PyC layer is close to isotropic and purely elastic [18]. The initial Young's modulus of SiC is given as 400 GPa from measurement of the SiC cross section. The output of the bending displacement from FE modelling will be used to obtain the indentation displacement at the external surface of the SiC (described later). The interface between the inner sphere and the outer shell is perfectly bonded. A three dimensional solid element, 4-node linear tetrahedron, is used to mesh the model.

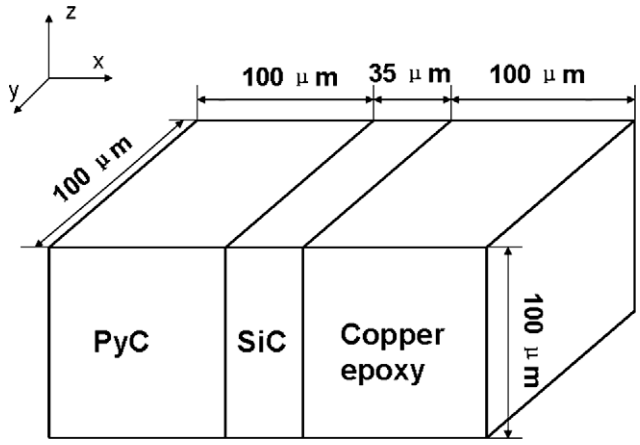

Fig. 4. A schema of the dimensions of a three-layered system (like a sandwich): PyC, SiC and Copper epoxy mounting compound for modelling.

In the model, it should be noted that the contact force will induce a large strain in the very local area nearby the indent. Such deformation caused by indentation needs to be decoupled from that caused by bending. To this end, an identical SiC bulk model is used as a calibration. When the SiC bulk model and the external surface of SiC coating are indented by identical applied force, bending happens in the SiC coating but is absent in the SiC bulk model. It is assumed that the two models share the same large local strain caused by the indentation force, therefore, when the displacement of the reference SiC bulk is subtracted from that of the SiC coating, the effect of the displacement induced by bending is obtained.

2.3. Nanoindentation experiment

Nano-indentation was carried with a Berkovich indenter in the nano-Indenter™ XP (MTS Systems Corp., USA). Calibration of Young's modulus was made with a standard silica specimen. The penetration depth for SiC layer was normally set a constant value as 500 nm (the contact depth is around 300 nm) in order to avoid size effect. This penetration depth is chosen because the depth should be large enough to ignore surface roughness influence but meanwhile it can not be too large in order to avoid possible cracks produced. All data were analyzed using the Oliver and Pharr method [19].

3. Results and discussion

3.1. Anisotropic SiC

For the SiC layer produced by chemical vapour deposition, the grains exhibit columnar structure and grow along the radial direction as shown in Fig. 5, with an average grain size of 4 μm × 500 nm. Since in the coated fuel particles, the main pressure comes from the kernel inside and push the SiC coating in the radial direction, the stresses in radial and orthoradial directions are both produced in the SiC coating. Therefore, the evaluation of Young's modulus of the SiC coating in radial and orthoradial directions will give access to normal radial and orthoradial stresses, thus, it is necessary to obtain the Young's modulus of silicon carbide in both directions.

Table 2
Dimensions and material properties of the FE model for indentation at the external surface of SiC.

	Inner radius (μm)	Outer radius (μm)	Distance between the external surface after polishing and the centre (μm)	Poisson's ratio	Young's modulus (GPa)
Inner sphere	–	400	–	0.17	28
Outer shell	400	435	422	0.25	442 (After correction)

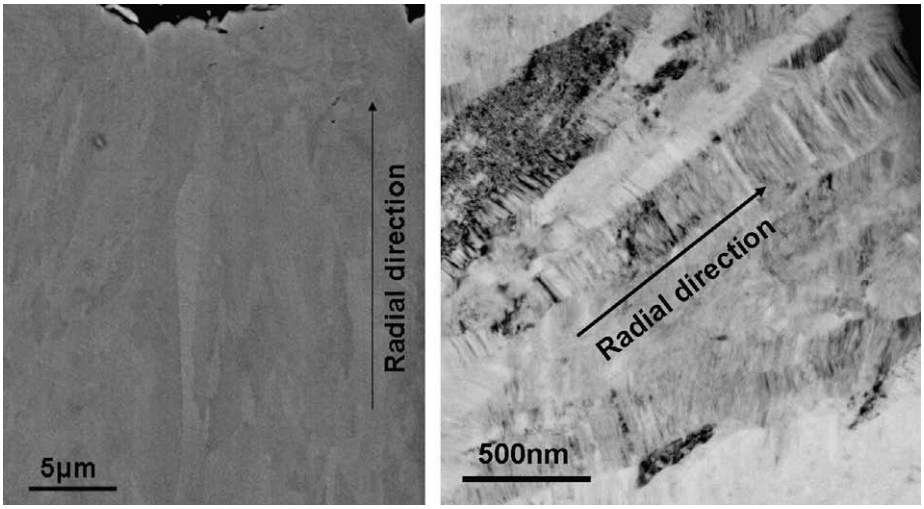

Fig. 5. The columnar SiC grains observed by SEM (left) and TEM (right).

3.2. Indentation on cross-section

From the contact stiffness data and Eqs. (1.1) and (1.2), the Young's modulus of the SiC layer is measured as 391.1 ± 12.9 GPa. As mentioned earlier, during the experimental process, the surface roughness effect and size effect are ignored by controlled polishing and setting an appropriate indentation depth. The key issue would be the effect of the adjacent layer on the SiC film because the modulus of the carbon layer is only around 28 GPa and the copper epoxy is about 37 GPa, which are both much lower than the modulus of SiC. As a result, a finite element modelling is introduced to analyze this influence. By using the material parameters listed above the indentation on cross-section is simulated (Table 3). The resulting indentation load–displacement curve in Fig. 6 shows that the theoretical indentation response not only agrees with experimental curve, but also agrees with that using a homogeneous bulk SiC specimen. The results confirm that both carbon layer and copper epoxy have little effect on indentation of SiC, and the obtained SiC modulus (about 391 GPa) is reasonable. In other words, the "substrate" effect is negligible in the present experiment.

Fig. 7 gives the Young's modulus obtained from continuous stiffness measurements on a homogeneous CVD 3C-SiC produced by Rohm&Hass Co. with 30 mm diameter × 7 mm and cross section of SiC, respectively. The homogeneous SiC bulk sample shows a standard continuous stiffness measurement profile where the measured Young's modulus is invariant with indentation depth. Interestingly, the cross section of SiC also shows a constant Young's modulus with respect to indentation depth, which further confirms the absence of the 'substrate' effect for indentation on cross-section, which is attributed to the fact that the indentation radius is much smaller than the SiC thickness, and the indented locations are far away from the interface between SiC and its neighbour materials.

Table 3
The modulus and Poisson ratio of each layer by modelling.

Material	Poisson ratio	Young's modulus (GPa)
SiC	0.25	400
Carbon	0.21	28
Copper epoxy	0.34	37

3.3. Indentation at external surface of SiC

Fig. 7 gives the Young's modulus from continuous stiffness measurements on the external surface, which shows a decreasing trend with increase in penetration depth. The contact stiffness as a function of penetration depth of the homogeneous SiC is compared

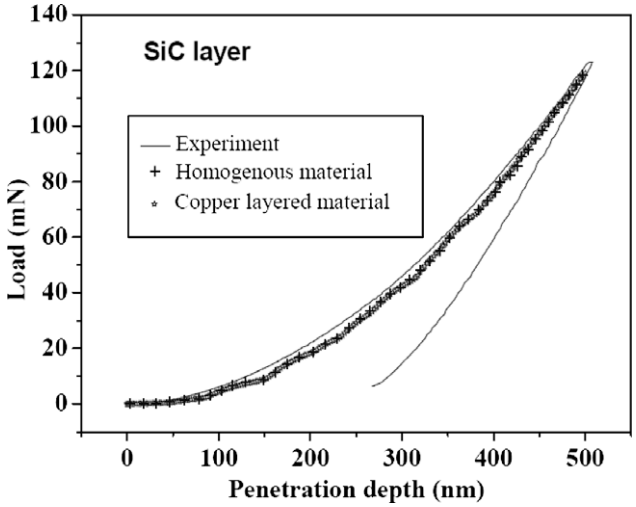

Fig. 6. On the cross section, the experimental and modelling load–displacement curves of SiC embedded in the copper epoxy compound comparing with homogenous SiC material.

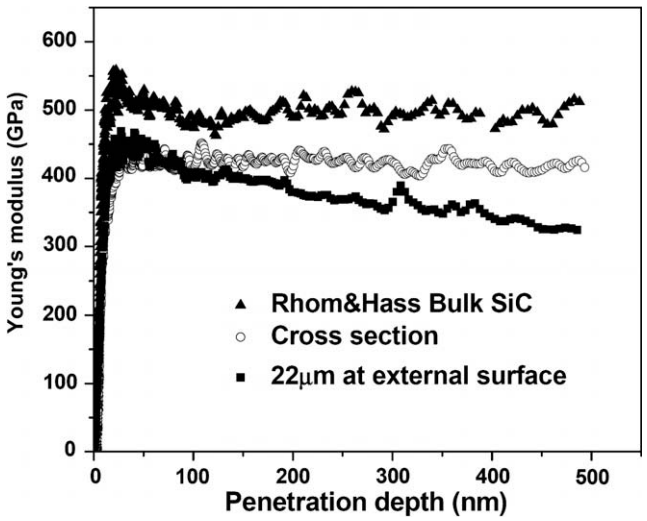

Fig. 7. The modulus curves of three SiC samples obtained by continuous stiffness measurement (The bulk SiC is from Rohm&Hass Co. and is 30 mm diameter × 7 mm in size).

with that indented on the cross section and external surface of SiC in Fig. 8. The stiffness profiles of external surface indentation shows that the contact stiffness trend is not linear, which indicates a possible substrate effect or bending effect upon indentation on the external surface. However, the thickness of SiC is 22 μm, much bigger than ten times of the indentation contact depth (300 nm), which according to Ref. [15], this system of SiC film on the carbon should roughly comply with one-tenth rule because their mismatch σ_{SiC}/σ_c is around 11.2/1.2 = 9.3. Here, σ_{SiC} is the yield stress of SiC film and σ_c is the yield stress of carbon. Therefore, Figs. 7 and 8 imply bending effect occurred rather than the substrate effect. The question is how much bending effect can be learned from Figs. 7 and 8.

Assuming elastic indentation with a sharp indenter, the applied force P and depth h_i can be related by $P = Ah_i^2$ (A is a constant) for a bulk material, and the contact stiffness would become $S_i = 2Ah_i$, and thus S_i varies linearly with h_i. When bending occurs, the bending displacement is very small due to the high Young's modulus of SiC and we can also assume the bending behaviour is purely elastic, as a result, $P = \lambda h_b$, with the bending stiffness denoted as $S_b = \lambda$ (λ is a constant). Here, h_b is displacement due only to bending.

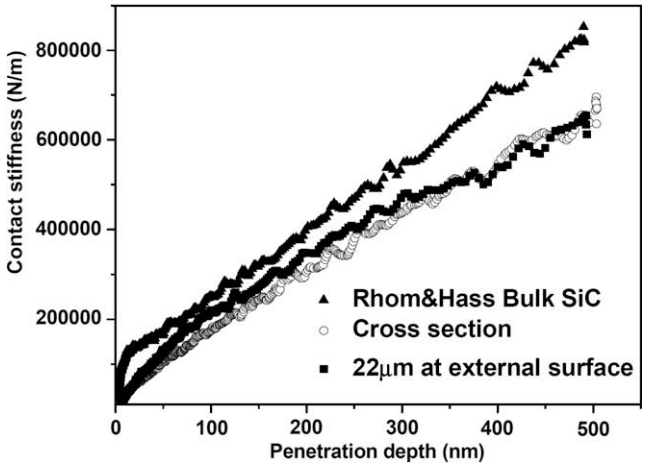

Fig. 8. Contact stiffness as a function of penetration depth for three samples by continuous stiffness measurement.

Assuming small deformation and the strains resulting from bending and indentation can be decoupled, the total displacement due to indentation at the external surface of the SiC layer should be

$$h_T = h_i + h_b \tag{3.1}$$

where h_T should be larger than h_i because bending happens in the same direction with indentation. Then the total stiffness is

$$S_T = \frac{dP}{dh_T} = \frac{dP}{d(h_i + h_b)} = \frac{1}{\frac{dh_i}{dP} + \frac{dh_b}{dP}} \tag{3.2}$$

As a result

$$S_T = \frac{2A\lambda h_i}{\lambda + 2Ah_i} \tag{3.3}$$

At the identical force P, we can have $\lambda h_b = Ah_i^2$, substituting h_T using Eq. (3.1), then $h_i = \frac{\lambda}{Ah_i + \lambda} h_T$, thus the Eq. (3.3) could be rewritten as

$$S_T = \frac{\lambda^2}{(\lambda + Ah_i)(\lambda + 2Ah_i)} \cdot 2Ah_T \tag{3.4}$$

Obviously, S_T deviates from the curve of $S_T = 2Ah_T$, so the total stiffness is not linear with the total depth h_T any more. Because $\frac{\lambda^2}{(\lambda + Ah_i)(\lambda + 2Ah_i)} < 1$, the value of S_T is always less than $2Ah_T$; when the depth increases, the deviation from $S_T = 2Ah_T$ is bigger. The Eq. (3.4) explains the stiffness-displacement curve from indentation of the SiC coating at the external surface (Fig. 8).

3.3.1. Young's modulus along the CVD growth direction

Since bending would affect Young's modulus measured, the measured Young's modulus from experiment would include indentation and bending contribution. To obtain Young's modulus of of SiC from indentation at external surface, contribution of the stiffness from bending should be separated from the indentation stiffness without bending. Then the stiffness and contact area from indentation are used to obtain Young's modulus according to the Eqs. (1.1) and (1.2).

3.3.1.1. Stiffness. The total stiffness should attribute to both indentation and bending, and it relates to

$$\frac{1}{S_T} = \frac{dh_i}{dP} + \frac{dh_b}{dP} = \frac{1}{S_i} + \frac{1}{S_b} \tag{3.5}$$

where h_T is the total displacement, and the subscripts i, b and T refer to indentation, bending and total contribution, respectively. Therefore, the indentation stiffness, which only comes from the indentation contribution, could be obtained after subtracting the bending stiffness as

$$\frac{1}{S_i} = \frac{1}{S_T} - \frac{1}{S_b} \tag{3.6}$$

Here, S_T can be measured from experiments, and $\frac{dP}{dh_b}$ is the bending stiffness S_b, which could be obtained by the FE calculation described in section IIB with an assumed Young's modulus of SiC. Fig. 9 shows the displacement from the FE modelling, which is around 89 nm. After justifying the assumed elastic bending behaviour, the bending displacement is about 35 nm. The bending stiffness S_b could be obtained as 3.8103×10^6 N/m, since the total stiffness in experiments is around 0.5590×10^6 N/m, using Eq. (3.6), the indentation stiffness S_i can be calculated out as 0.6560×10^6 N/m.

3.3.1.2. Contact area estimation. Fig. 10 shows the schematic of indentation profile of SiC with and without bending contribution. When the film is bent, $P = \lambda h_b$ and the displacement is purely elastic, thus bending should not affect the residual depth h_f, therefore $h_{Tf} = h_{if}$, where h_{Tf} and h_{if} represents the total residual depth and indentation residual depth, respectively.

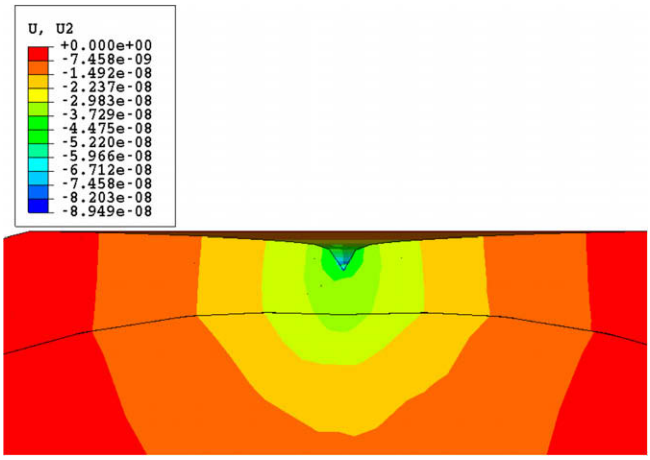

Fig. 9. The displacement under the indentation force using FE modelling on the external SiC surface, the bending displacement should use this maximum displacement to subtract the displacement in the bulk SiC material (54 nm) under the identical force in order to correct large strain induced by contact force. The outer layer is SiC and inner layer is carbon.

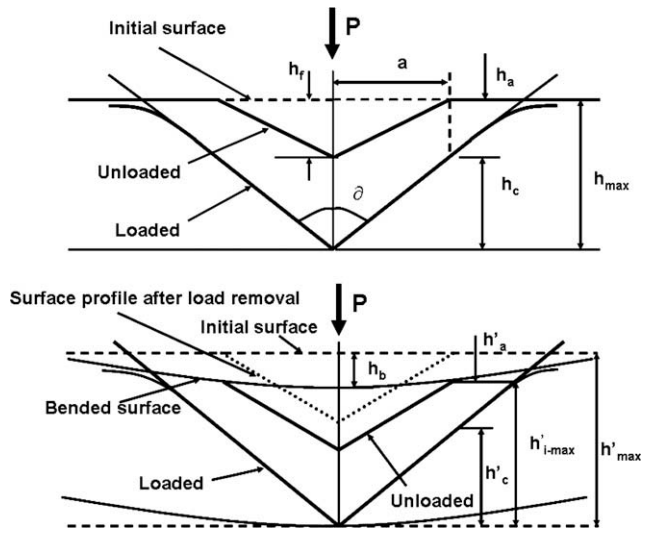

Fig. 10. The schematic of indentation without (top) and with bending (down) for contact area calculation on the external surface of SiC.

For indentation without bending, according to Sneddon's calculation [20] based on the elastic half space, as an axis-symmetric cone, at any time during loading, the force could be written as

$$P = \frac{\pi}{2} E_r a^2 \cot\alpha \tag{3.7}$$

And the penetration displacement is

$$h_i = \frac{\pi}{2} a \cot\alpha \tag{3.8}$$

where α is the semi-angle of the indenter, E_r is the reduced modulus, a is the contact radius. Combining these two equations, the load and displacement can be related by

$$P = \left(\frac{2E_r}{\pi}\tan\alpha\right) h_i^2 \tag{3.9}$$

The force is proportional to h^2 for the loading curve as we mentioned previously, and the indentation stiffness is given by

$$S_i = \frac{dP}{dh_i} = \frac{4E_r \tan\alpha}{\pi} h_i \tag{3.10}$$

The indentation contact stiffness is linear with the displacement. Substituting Eq. (3.10) into Eq. (3.9), we obtain:

$$h_i = \frac{2P}{dP/dh_i} \tag{3.11}$$

The above equations are generated from the loading curve of indentation, which include both elastic and plastic behaviour. When the load reaches the peak load, the load and displacement are P_{max} and h_{max}, respectively. During unloading, the elastic deformation is fully recovered but plastic deformation remains; the final depth of residual impression is h_{if}. Thus unloading part is elastic and the displacement should be h_i-h_{if} rather than h_i by itself according to Sneddon's expression [21], which only applies to the elastic component of the displacement, so the Eq. (3.11) could be changed as

$$h_i - h_{if} = \frac{2P}{dP/dh_i} \tag{3.12}$$

For the conical indenter, based on Sneddon's analytical solution [21], the contact depth can be expressed as

$$h_{ic} = h_{i\max} - \frac{\pi - 2}{\pi}(h_i - h_{if}) \tag{3.13}$$

The contact depth has the relationship with h_{imax} as

$$h_{ic} = h_{i\max} - h_{ia} \tag{3.14}$$

Combining with Eqs. (3.12)–(3.14), we obtain

$$h_{ic} = h_{i\max} - \frac{2(\pi - 2)}{\pi}\frac{P}{dP/dh_i} \tag{3.15}$$

Considering both bending and indentation, the total penetration depth at the maximum force should be

$$h_{T\max} = h_{i\max} + h_b \tag{3.16}$$

So the Eq. (3.15) can be rewritten as

$$h_{ic} = h_{T\max} - h_b - \frac{2(\pi - 2)}{\pi}\frac{P}{dP/dh_i} \tag{3.17}$$

Then the contact area of indentation contribution only could be obtained

$$A_{ic} = \pi a^2 = \pi(h_{ic}\tan\partial)^2 = 24.5 h_{ic}^2 \tag{3.18}$$

The values of $h_{T\max}$ and P can be obtained from experiments, the bending displacement could be extracted by FE modelling, and the indentation stiffness $\frac{dP}{dh_i} = S_i$ is obtained in Section 3.3.1.1.

3.3.1.3. Calibration of Young's modulus. After obtaining both indentation stiffness and contact area as described in Sections 3.3.1.1 and 3.3.1.2, the Young's modulus can be calculated according to Eq. (1.1). With a corrected input value of 442 GPa as SiC Young's modulus for calculation of bending displacement using FE modelling, then the calculation according to Eq. (1.1) gives 442.5 GPa as the Young's modulus of SiC from indentation at external surface of the SiC (Table 4). The procedure to obtain this value is described as follows.

When the bending displacement is calculated using FE modelling initially (section IIB), an initial Young's modulus of 400 GPa (It is noted that 391 GPa was obtained from indentation at cross-section) was given at first. Then following the procedures described in Sections 3.3.1.1 and 3.3.1.2 to obtain both indentation stiffness and contact area, the Young's modulus of 445 GPa is obtained according to Eqs. (1.1) and (1.2). Therefore, a mean value of 420 GPa is used for calculation of bending displacement again, followed by calculation of Young's modulus according to Eqs. (1.1) and (1.2). After such calculation cycles, Young's modulus of

Table 4
Some data in calculation procedure of Young's modulus.

Bending displacement (nm)	Bending stiffness ($\times 10^6$ N/m)	Experimentally measured stiffness ($\times 10^6$ N/m)	Calculated indentation stiffness ($\times 10^6$ N/m)	Contact area (nm^2)	Young's Modulus (GPa)
35.01	3.8103	0.5590	0.6560	3431124	442.5

442 GPa is obtained as both input data for calculation of bending displacement and output data of Eqs. (1.1) and (1.2), which we believe is the Young's modulus of SiC along the CVD direction. It should be noted here that there could be some error in this value as the bending displacement is calculated based on FE modelling without experimental confirmation due to limitations. Nevertheless, the value is reasonable because the calculation of bending displacement in modelling is dependent on the ratio of Young's modulus of SiC and Carbon rather than SiC film only.

3.4. Young's modulus of SiC parallel and vertical to CVD growth direction

From indentation on the external surface of SiC, the Young's modulus is evaluated to be 442.5 ± 13.3 GPa, the associated experimental uncertainty is gathered from more than 20 experimental measurements. The minor uncertainty probably is due to the surface roughness and defects in the SiC sample. This modulus value is higher than Young's modulus of 391.1 ± 12.9 GPa measured from indentation at the cross section. This implies that the SiC layer is anisotropic in terms of mechanical properties. Both SEM and TEM observations show that SiC grains are of columnar structure (Fig. 5), with an average grain size of 500 nm × 3 μm. Here nanoindentation experiments give indentation modulus rather than conventional Young's modulus. The indentation modulus is a local elastic property, in this case, the indentation size is around 3 μm which may cover several columns. Therefore, the measured modulus could be affected by grain orientation, grain size and grain boundary. As a result, a possible explanation of higher modulus along the column axial direction is that SiC grains sliding should be more difficult because of longer grain boundary which induces bigger grain boundary friction when comparing with vertically to growth direction [22,23] (Fig. 11). The other reason is probably when nanoindentation is performed on the grains, most of cracks induced by indentation are along the grain boundary, the longer grain boundary paralleling the column grain, the more difficultly grain boundaries are broken by these cracks (Fig. 12). Therefore, the modulus is measured higher than the other direction.

Another possible reason is that the modulus in the direction paralleled to grain growth is along the closely-packed ⟨1 1 1⟩ direction [24], and therefore leads to a higher Young's modulus value. Similar phenomenon was observed in pure copper using nanoindentation by ZD Guo et al [25]. It was found that the nearer the ⟨1 1 1⟩ direction, the Young's modulus is higher than that nearer the ⟨0 0 1⟩ direction.

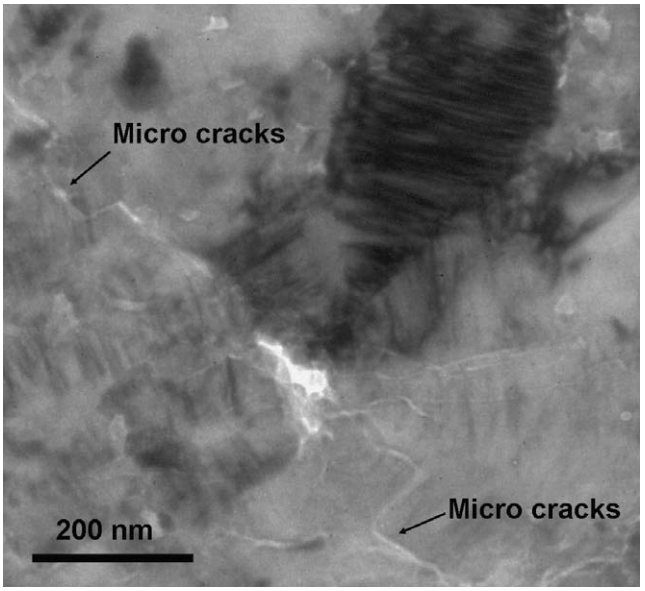

Fig. 12. Most cracks induced by indentation are along the grain boundary.

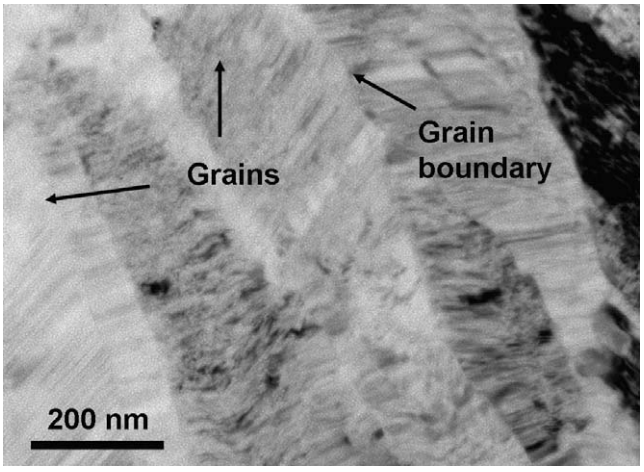

Fig. 11. Grains and grain boundary of SiC in high maginification TEM (The grain sliding can be possible happened in the nanoindentation experiment).

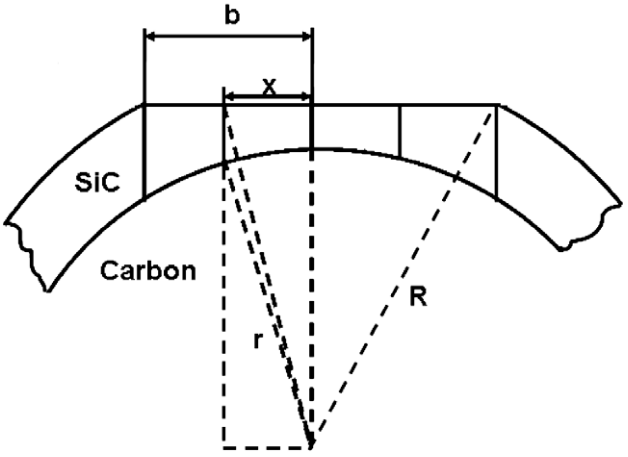

Fig. 13. The schematic of spherical SiC film on the carbon for the angle calculation. (R – the radius of the whole particle, r – the radius of the whole particle excluding SiC film, b – the radius of polished external surface, x – the distance from the centre of polished external surface, the angle of column grain orientation and indentation is arcsin (x/R)).

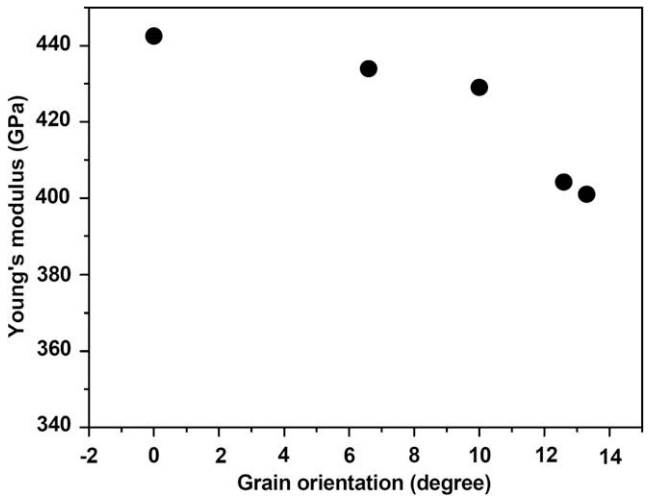

Fig. 14. The Young's modulus of SiC layer measured from the external surface as a function of grain orientation angles.

3.5. The effect of grain orientation on the modulus

When indentation is carried on the external surface of the SiC layer, the angle between indentation direction and column length direction varies from zero degree at the centre of the polished surface to 14 degree at a distance of 110 μm away from the centre. Fig. 13 shows the schematic of indentation vs SiC column orientation with minimum thickness of SiC as 22 μm for the orientation angle calculation. Fig. 14 shows the Young's modulus as a function of SiC column orientations. The Young's modulus decreases with increase in the angle, which agrees with the fact that the highest Young's modulus is along the column length direction.

4. Conclusions

Indentation tests are carried out on both the external surface and cross-section of SiC layer. Bending occurs with indentation on the external surface of the SiC layer, while bending displacement is simulated using a FE model. Taking bending into account, the Young's modulus of SiC is obtained as 442.5 ± 13.3 GPa from indentation on the external surface. On the other hand, Young's modulus of SiC is obtained as 391.1 ± 12.9 GP from indentation at the cross-section. The difference between the two Young's moduli can be explained due to anisotropic microstructure of the SiC layer, i.e. the columns grow along the radial direction of the spherical coated particle. It is also found that the Young's modulus decreases with the increase of the column/indentation angle. Although there may be some error in this method to obtain Young's modulus of SiC, the study provides a method to measure mechanical properties of the SiC layer within such complex geometry and anisotropic microstructure. Such method can be extended to measurements of other similar systems.

Acknowledgements

The authors would like to thank A. Forrest at School of Materials, University of Manchester for his help on nanoindentation experiments and British Nuclear Fuel Ltd. (Now Nexia Solutions) for financial support.

References

[1] L.L. Snead, T. Nozawa, Y. Katoh, T.-S. Byun, S. Kondo, D.A. Petti, J. Nucl. Mater. 371 (2007) 329–377.
[2] R.J. Price, Nucl. Technol. 35 (1977) 320.
[3] K. Bongartz, E. Gyarmati, H. Schuster, K. Tauber, J. Nucl. Mater. 62 (1976) 123.
[4] S.J. Xu, J.G. Zhou, B. Yang, B.Z. Zhang, J. Nucl. Mater. 224 (1995) 12.
[5] B.V. Cockeram, J. Am. Ceram. Soc. 85 (2002) 603.
[6] K. Bongartz, E. Gyarmati, H. Nickel, H. Schuster, W. Winter, J. Nucl. Mater. 45 (1972) 261.
[7] S.G. Seshardri, K.-Y. Chia, J. Am. Ceram. Soc. 70 (1987) C-242–C-244.
[8] T.D. Gulden, J. Am. Ceram. Soc. 52 (1969) 585.
[9] C. Bellan, J. Dhers, Thin Solid Films 469–470 (2004) 214.
[10] X. Zhao, R.M. Langford, J. Tan, P. Xiao, Script. Materialia. 59 (2008) 39.
[11] A.C. Fischer-Cripps, Surf. Coat. Technol. 200 (2006) 4153.
[12] M. Zhao, X. Chen, Y. Xiang, J.J. Vlassak, D. Lee, Acta Materialia 55 (2007) 6260.
[13] T.Y. Tsui, J. Vlassak, W.D. Nix, J. Mater. Res. 14 (1999) 2204.
[14] J.A. Knapp, D.M. Follstaedt, S.M. Myers, J.C. Barbour, T.A. Friedmann, J. Appl. Phys. 85 (1999) 1460.
[15] X. Chen, J.J. Vlassak, J. Mater. Res. 16 (2001) 2974.
[16] J.L. He, S. Veprek, Surf. Coat. Technol. 163–164 (2003) 374.
[17] E. López-Honorato, P.J. Meadows, J. Tan, P. Xiao, J. Mater. Res. 23 (2008) 1785.
[18] E. López-Honorato, P.J. Meadows, P. Xiao, G. Marsh, T.J. Abram, Nucl. Eng. Des. 238 (2008) 3121.
[19] W.C. Oliver, G.M. Pharr, J. Mater. Res. 7 (1992) 1564.
[20] I.N. Sneddon, in: Proceedings of the Cambridge Philosophical Society, vol. 44, 1948, p. 492.
[21] I.N. Sneddon, Int. J. Eng. Sci. 3 (1965) 47–57.
[22] S. Bhowmick, Z.-H. Xie, M. Hoffman, V. Jayaram, S.K. Biswas, J. Mater. Res. 19 (2004) 2616.
[23] S.J. Suresha, R. Gunda, V. Jayaram, S.K. Biswas, J. Mater. Res. 22 (2007) 3501.
[24] Y. Kajikawa, S. Noda, H. Komiyama, Chem. Vapor. Deposit. 8 (2002) 99.
[25] Z. Guo, X. Wang, X. Yang, D. Jiang, X. Ma, H. Song, Acta Metallurgica Sinica 44 (2008) 901.